

The Raman response of double wall carbon nanotubes

F. Simon, R. Pfeiffer, C. Kramberger, M. Holzweber, and H. Kuzmany
Institute of Materials Physics, University of Vienna, A-1090 Vienna, Strudlhofgasse 4., Austria

Raman spectroscopy on carbon nanotubes (CNT) yields a rich variety of information owing to the close interplay between electronic and vibrational properties. In this paper, we review the properties of double wall carbon nanotubes (DWCNTs). In particular, it is shown that SWCNT encapsulating C₆₀, so-called peapods, are transformed into DWCNTs when subject to a high temperature treatment. The inner tubes are grown in a catalyst free environment and do not suffer from impurities or defects that are usually encountered for as-grown SWCNTs or DWCNTs. As a consequence, the inner tubes are grown with a high degree of perfection as deduced from the unusually narrow radial breathing mode (RBM) lines. This apostrophizes the interior of the SWCNTs as a nano-clean room. The mechanism of the inner nanotube production from C₆₀ is discussed. We also report recent studies aimed at the simplification and industrial scaling up of the DWCNT production process utilizing a low temperature peapod synthesis method. A splitting of the RBMs of inner tubes is observed. This is related to the interaction between the two shells of the DWCNTs as the same inner tube type can be encapsulated in different outer ones. The sharp appearance of the inner tube RBMs allows a reliable assignment of the tube modes to (n,m) indexes and thus provides a precise determination of the relation between the tube diameter and the RBM frequencies.

INTRODUCTION

Carbon nanotubes have been in the forefront of the nanomaterial research since their discovery [1]. They are not only fundamentally interesting materials due to their appealing one-dimensional structure but several applications have been envisaged. Some of them have already been established such as scanning probe-heads [2] or field emission devices [3][4]. There is an active ongoing work in these fields to exploit the properties of these materials better and to improve the device qualities. Furthermore, high expectations are related to their applications as building elements of electronics, composite reinforcing materials and many more.

Carbon nanotubes can be represented as rolled up graphene sheets, i.e. single layers of graphite. Depending on the number of coaxial carbon nanotubes, they are usually classified into multi-wall carbon nanotubes (MWCNTs) and single wall carbon nanotubes (SWCNTs). Some general considerations have been clarified in the last 13 years of nanomaterial research related to these structures. MWCNTs are more homogeneous in their physical properties as the large number of coaxial tubes smears out individual tube properties. This makes them suitable candidates for applications where their nanometer size and the conducting properties can be exploited. In contrast, SWCNT materials are grown as an ensemble of weakly interacting tubes with different diameters. The physical properties of similar diameter SWCNTs can change dramatically as the electronic structure is very sensitive on the rolling-up direction, the so-called chiral vector. Depending on the chiral vector, SWCNTs can be metallic or semiconducting [5]. This provides a richer range of physical phenomena as compared to the MWCNTs, however significantly limits the range of applications. To date, neither the directed growth nor the controlled selection of SWCNTs with a well defined chiral vector has been performed successfully. Thus, their broad applicability is still awaiting. Correspondingly, current research is focused on the post-synthesis separation of SWCNTs with a narrow range of chiralities [6][7][8][9] or on methods which yield information that are specific to SWCNTs with different chiralities. An example for the latter is the observation of chirality selective band-gap fluorescence in semiconducting SWCNTs [10].

A more recently discovered third class of CNTs are double-wall carbon nanotubes (DWCNTs). DWCNTs were first observed to form under intensive electron radiation [11] in a high resolution transmission electron microscope from C₆₀ encapsulated in SWCNTs, so-called peapods [12]. Following the synthesis of C₆₀ peapods in macroscopic amounts [13], bulk quantities of the DWCNT material are available using a high temperature annealing method [14]. Alternatively, DWCNTs can be produced with usual synthesis methods such as arc-discharge [15] or CVD [16] under special conditions. According to the number of shells, DWCNTs are between SWCNTs and MWCNTs. Thus, one expects that DWCNTs may provide a material where improved mechanical stability as compared to SWCNTs coexists with the rich variety of electronic properties of SWCNTs. There are, of course, a number of yet unanswered questions e.g. if the outer tube properties are unaffected by the presence of the inner tube or if the commensurability of the tube structures plays a role. These questions should be answered before the successful application of these materials.

In this contribution, we review Raman studies of DWCNTs. We show that the study of inner tubes, in particular those from C₆₀ peapod based DWCNTs provides some unique insight into the physics of SWCNTs. Such studies enabled the observation of unprecedently sharp Raman modes, which evidence that the inside grown SWCNTs are

higly perfect mainly due to the catalyst free nano-clean room interior of outer SWCNT reactor tubes. The sharp Raman features of inner tube Raman radial breathing modes (RBMs) enable the indexing of chiral vectors thus providing a simple alternative to the band-gap fluorescence method.

This review is organised as follows: we describe the experimental methods and the sample preparation that are used for the current study. We compare the properties of DWCNTs grown with different methods. We show that the C₆₀ peapod based DWCNTs have unique properties which underline the nano-clean room conditions encountered in the inside of SWCNTs. We describe a novel method for the preparation of the C₆₀ peapod precursor material that enables the large scale productions of DWCNTs. We present a detailed investigation of the electronic structure of the small diameter inner tubes. We also present the chiral vector assignment to such tubes thus refining the empirical parameters of the relation between the RBM frequencies and the tube diameters.

EXPERIMENTAL

SWCNT starting materials for the production of DWCNTs described herein were prepared by the laser ablation method. Their diameters were controlled in order to obtain efficient C₆₀ encapsulation that results in high yield of inner nanotubes. The values of $d_L = 1.39$ nm, $\sigma_L = 0.1$ nm were obtained for the mean diameter and the variance of the distribution for the different samples using a large number of exciting laser energies following Ref. [17]. The SWCNT materials were purified following Ref. [13]. Peapod samples were prepeared by annealing SWCNTs with C₆₀ in a quartz ampoule following Ref. [13]. The peapod filling fraction was close to 100% as evidenced previously on similar samples using Electron Energy Loss Spectroscopy (EELS) [18]. The peapod materials were transformed to DWCNTs using the high temperature annealing method of Ref. [14]. The samples in the form of bucky-paper are kept in dynamic vacuum and on a copper tip attached to a cryostat, which allows temperature variation in the 20-600 K temperature range. The Raman experiments were performed in a 180 degree backscattering geometry. A He/Ne, an Ar/Kr mixed gas, and a tunable Ti:sapphire laser pumped by an Ar laser were used for the excitation at 30 different laser lines. Multi frequency Raman spectroscopy was performed on a Dilor xy triple axis spectrometer in the 1.64-2.54 eV (755-488 nm) energy range and in a Bruker FT-Raman spectrometer for the 1.16 eV (1064 nm) excitation at 90 K. We operated the Dilor spectrometer in two modes, high and normal resolution. The high resolution uses the additive mode of the spectrometer and the spectral resoluton as determined from the FWHM of the elastically scattered light was 0.4-0.7 cm⁻¹ going from red to blue excitation. Similarly, spectral resolution in the normal mode was 1-2 cm⁻¹ depending on the laser line. Measurements with the FT-Raman spectrometer were recorded with 1 cm⁻¹ resolution. Raman shifts were accurately calibrated against a series of spectral calibration lamps. *Ab initio* calculations were performed with the Vienna Ab Initio Simulation Package (VASP) [19].

RESULTS AND DISCUSSION

DWCNT synthesis

Double-wall carbon nanotubes can be classified into two groups depending on the method used for their production. DWCNT samples produced with usual preparation methods [15] have less controllable parameters such as their diameter distributions and, as shown below, their quality is inferior compared to the C₆₀ peapod based DWCNTs. Following the discovery of DWCNTs from C₆₀ peapods under intensive electron irradiation [11], it was demonstrated using HR-TEM that a 1200°C heat treatment can also efficiently produce the inner nanotubes based on the C₆₀ peapods [20]. The first characterization of bulk amounts of DWCNTs produced by this synthesis method was performed using Raman spectroscopy by Bandow et al. [14].

In Fig. 1 we show a typical HR-TEM micrograph of C₆₀ peapod based DWCNT. The difference in the outer and inner tube diameter is thought to be close to twice the van der Waals distance of graphite, 0.335 nm. Indeed, X-ray studies have indeed shown that the inner and outer tube diameter difference is only slightly larger, 0.72±0.02 nm [21]. The corresponding situation for a DWCNT sample with outer tube distibution centered at the (10,10) tube is depicted in Fig. 2. The cut-off observed at small diameter inner tubes is given by the smallest outer tube diameter of 1.2 nm which allows the precursor C₆₀ to enter [22][23][24].

The transformation from C₆₀ peapods to DWCNTs can be conveniently followed by Raman spectroscopy. In Fig. 3 we compare the Raman spectra of pristine SWCNTs, C₆₀@SWCNT peapods, and DWCNTs based on the peapod material. The emergence of additional vibrational modes in the 200-450 cm⁻¹ spectral range is evident in Fig. 3 for the DWCNT material as compared to the pristine and peapod materials. This emergence is accompanied by

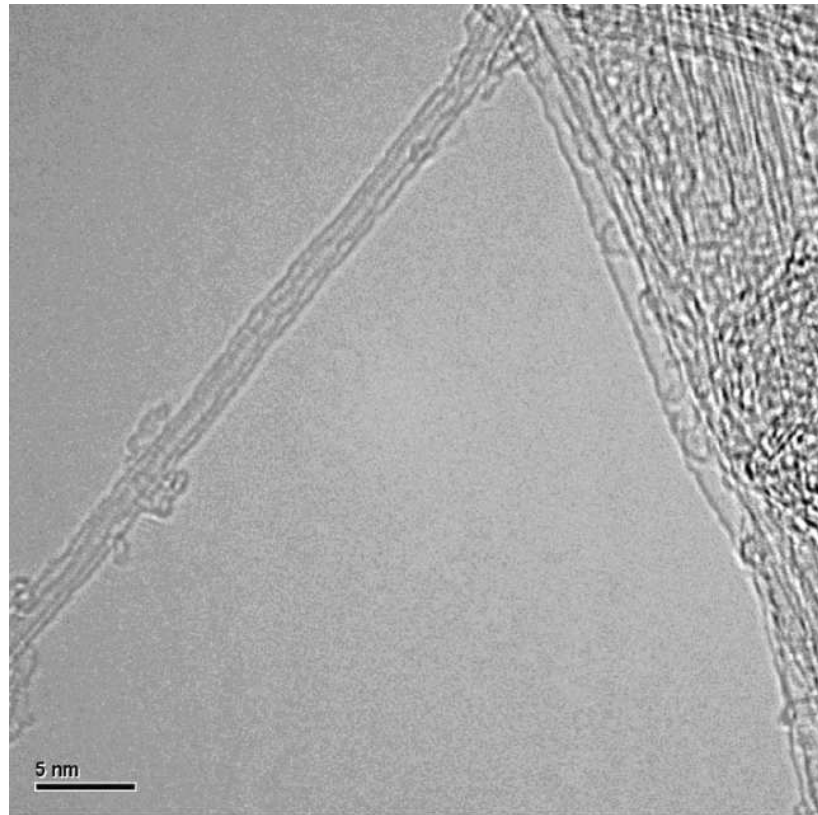


FIG. 1: High-resolution TEM micrograph of a C_{60} peapod based DWCNT sample.

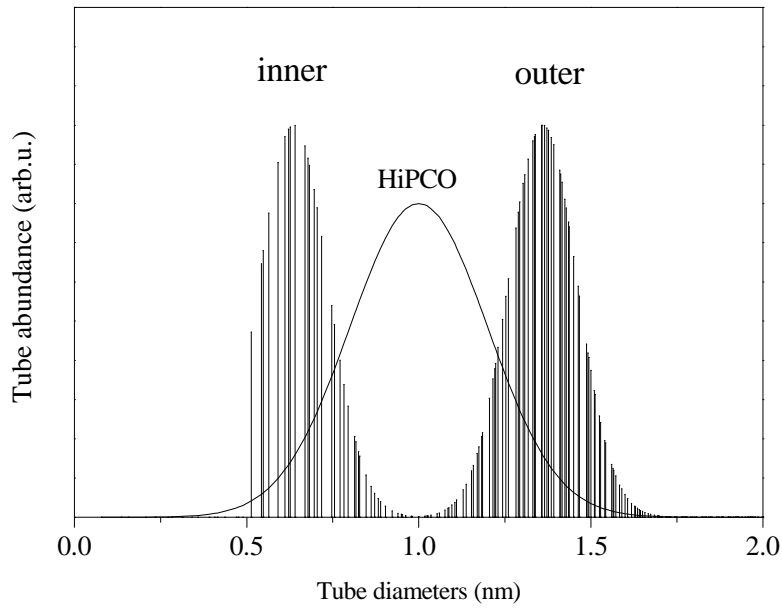


FIG. 2: Schematic diameter distribution of geometrically allowed tubes in the DWCNTs of the current study. The envelope of the approximate diameter distribution in a HiPco sample is shown for comparison.

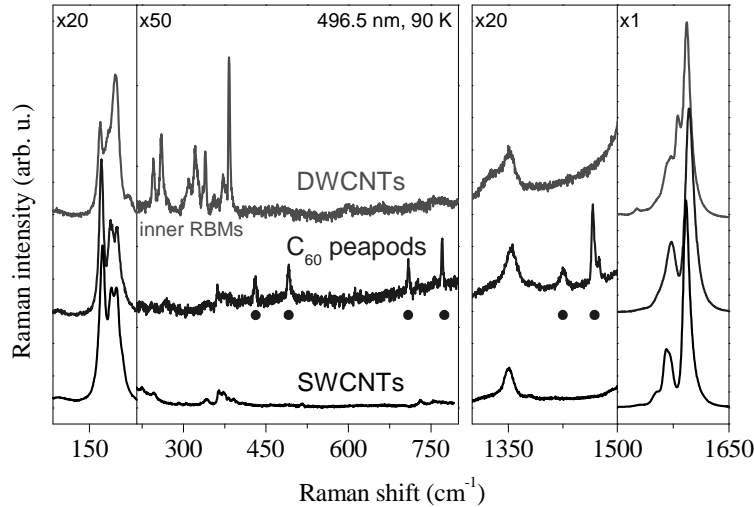


FIG. 3: Raman spectra of pristine SWCNT, C_{60} peapod and C_{60} peapod based DWCNT samples for $\lambda=497$ nm laser excitation and 90 K. Bullets mark the positions of the modes of encapsulated C_{60} .

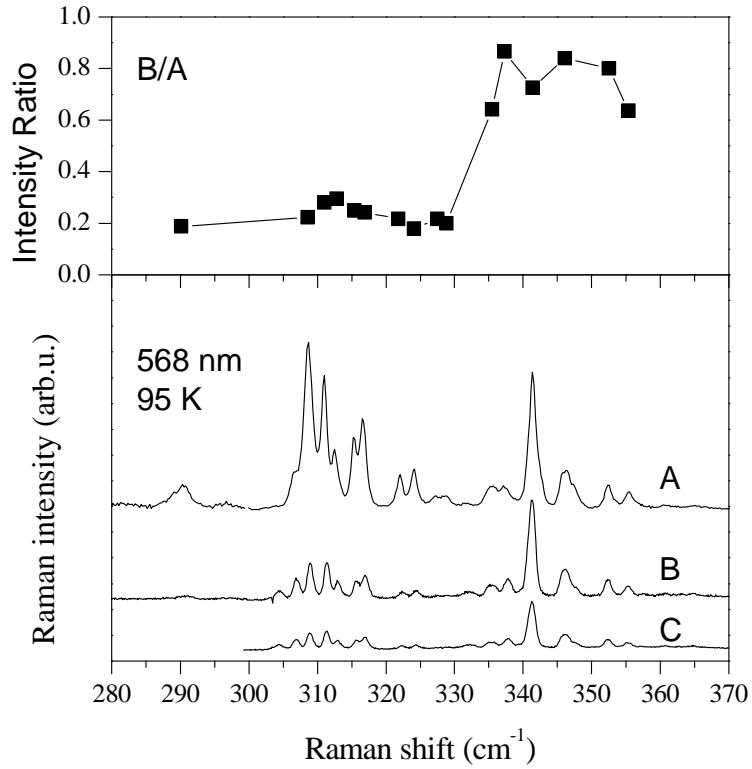


FIG. 4: Diameter selective growth of inner tubes in C_{60} peapod based DWCNT measured at $\lambda=568$ nm laser excitation.

the disappearance of the modes of the encapsulated fullerene as denoted by circles in Fig. 3. The extra lines in the $200-450\text{ cm}^{-1}$ spectral range were identified as the radial breathing modes of the smaller diameter inner shell tubes. The disappearance of the fullerene peaks is evidence that the encapsulated C_{60} serves as carbon source for the internal tube formation [14][25].

The inverse relationship between the RBM frequencies and tube diameters allows a tube diameter selective study of inner tube growth. In Fig. 4 we show the diameter selective growth of inner tubes. The topmost curve, A, shows the

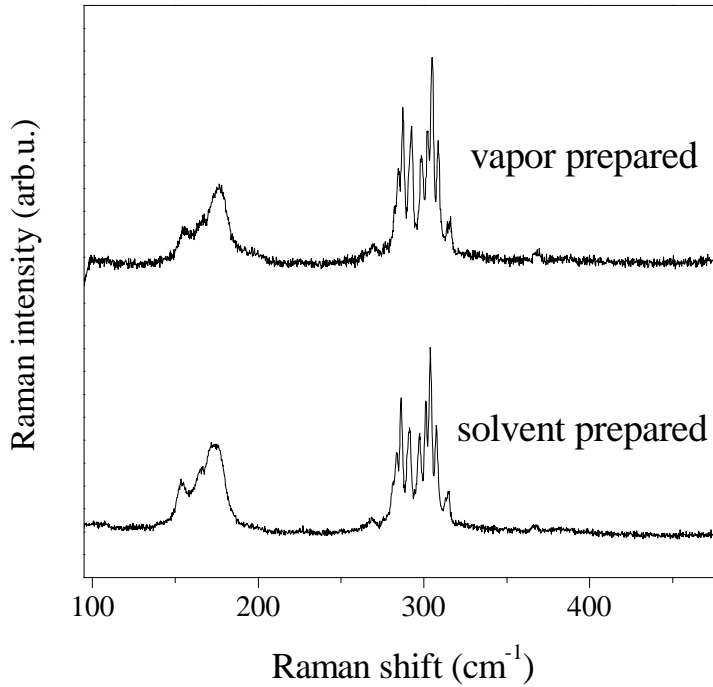


FIG. 5: Comparison of DWCNTs formed from vapor prepared (upper curve) and solvent prepared (lower curve) peapod samples at $\lambda=676$ nm laser excitation and room temperature.

fully developed inner tube RBM spectrum after a 12 h annealing at 1280°C annealing, whereas B and C correspond to 0.5 and 1 hour annealing. The comparison reveals the more rapid development of small diameter inner tubes, followed by the slower development of larger diameter tubes [26]. Similar diameter selective growth of inner tubes was found by Bandow et al. [27]. In the latter work, it was concluded from measurements at two laser excitations that small diameter inner tubes form first and are subsequently transformed to larger diameter inner tubes. This observation is somewhat different from the one reported here. The difference might be related to the photoselective property of the Raman experiments, as the data reported here are based on measurements on a larger number of laser lines. The formation of smaller tubes in the beginning, followed by the development of larger diameter tubes later on provides useful input for the theories aimed at explaining the inner tube formation. From computer simulation it was demonstrated that C₆₀ peapod based DWCNTs are formed by Stone-Wales transformations from C₆₀ dimer precursors formed at high temperature by cyclo-addition [28][29]. The free rotation of C₆₀ molecules is a prerequisite for the dimer formation as it enables the molecules to have facing double bonds. It has been found experimentally that the ellipsoidal shaped C₇₀ are present as both "standing" or "lying" peapod configurations i.e. with the longer C₇₀ axis perpendicular or parallel to the tube axis [30]. In small diameter tubes the lying C₇₀ configuration is preferred and the molecules have facing pentagons and consequently no cyclo-additional double bond formation is possible in a linear chain. For such small diameter tubes, dimers may be formed in a canted C₇₀ configuration. However this structure has not been observed experimentally. Experiments with C₇₀ peapod based DWCNTs have shown that inner tubes can indeed be formed from lying C₇₀ peapods, which presents a challenge to the current theories [31]. Clearly, more theoretical work is required on the formation process of inner tubes from fullerene peapod samples.

Apart from the lack of full understanding of the inner tube growth, the production process of the precursor fullerene peapods is relatively complicated and its scaling up to larger amounts is difficult. The usual, vapor filling, process involves the annealing of the fullerene together with the opened SWCNT material sealed together in a quartz ampoule. Recently, a new fullerene encapsulation technique involving the refluxing of the SWCNTs and the fullerenes in solvents was presented [32]. In Fig. 5 we show the comparison of DWCNT samples based on vapor and solvent filled C₆₀ peapods. Clearly, the yield and diameter distribution of the inner tubes are identical in the two kinds of samples which proves that the solvent filling method is indeed a simple alternative to the vapor filling method. In contrast to the latter, it can be easily scaled up to commercial quantities.

Production of DWCNTs has been reported by direct methods [15][16]. Such DWCNTs are characteristically different

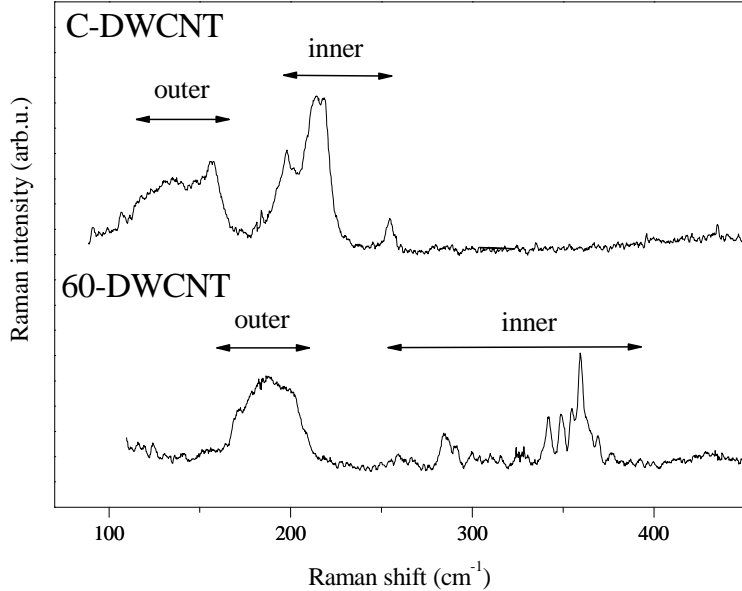


FIG. 6: Comparison of CVD grown (C-DWCNT) and C_60 peapod based DWCNT (60-DWCNT) materials at $\lambda=633$ nm laser excitation. Arrows indicate the Raman shift regions where RBMs of the outer and inner tubes are observed. The difference in inner and outer tube diameters in the two samples is apparent.

from the tubes grown from the peapod precursors. In Fig. 6 we show the comparison of directly produced (C-DWCNT) and C_60 peapod based DWCNT (60-DWCNT) materials. The C-DWCNTs were made from the catalytic decomposition of methane and was studied in detail previously [33]. There are clear similarities and differences in the comparison of the two kinds of DWCNT materials. Among the similarities, the Raman spectra of both compounds show two groups of bands. The lower frequency extending from $110-160\text{ cm}^{-1}$ for the C-DWCNT and from $165-200\text{ cm}^{-1}$ for the 60-DWCNT corresponds to the RBMs of the outer tubes. The modes seen at $190-250$ for the C-DWCNT and at $250-370\text{ cm}^{-1}$ for the 60-DWCNT correspond to the RBMs of the inner tubes. The difference in the observed RBM Raman shifts is related to the different diameters of the inner and outer tubes in the C-DWCNT and 60-DWCNT compounds. It was found that C-DWCNT material shown in Fig. 6 has $d_{\text{inner}} = 1.52\text{ nm}$, $\sigma_{\text{inner}} = 0.6\text{ nm}$, and $d_{\text{outer}} = 2.26\text{ nm}$, $\sigma_{\text{outer}} = 0.4\text{ nm}$ for the mean and the variance of the diameter distributions of the inner and outer tubes, respectively [16]. For the 60-DWCNT sample $d_{\text{inner}} = 0.67\text{ nm}$, $\sigma_{\text{inner}} = 0.1\text{ nm}$, and $d_{\text{outer}} = 1.39\text{ nm}$, $\sigma_{\text{inner}} = 0.1\text{ nm}$ was found [25]. The most important difference between the two materials is the smaller inner tube RBM linewidths for the 60-DWCNT sample. In what follows, we discuss the properties of only the peapod based 60-DWCNT samples and will refer to these briefly as DWCNTs.

Energy dispersive Raman studies of DWCNTs

Electronic structure of DWCNTs

The diverging behavior of the electronic density of states of SWCNTs gives rise to a significant resonant Raman enhancement and a photoselective Raman scattering. The photoselectivity, combined with the multi-frequency Raman method enables a detailed study of the electronic structure of the SWCNTs. The photoselective scattering also holds for the inner tubes of the DWCNTs. The laser energy dependent response of the inner tube RBMs is shown in Fig. 7. For the red excitation RBM linewidths as small as 0.35 cm^{-1} were observed [25]. This is almost an order of magnitude smaller than reported previously on individual SWCNTs [34]. Related to the narrow linewidth of the vibrational modes, the resonant excitation for several lines is significant, resulting in Raman intensities almost 10 times larger than those from the outer tubes. This implies very sharp resonances between the Van Hove singularities. This issue is discussed in detail below. In addition to the sharp electronic resonances, the electron-phonon coupling is enhanced for small diameter tubes [35], which may also contribute to the observed signal enhancement of the inner tube vibrational modes [25].

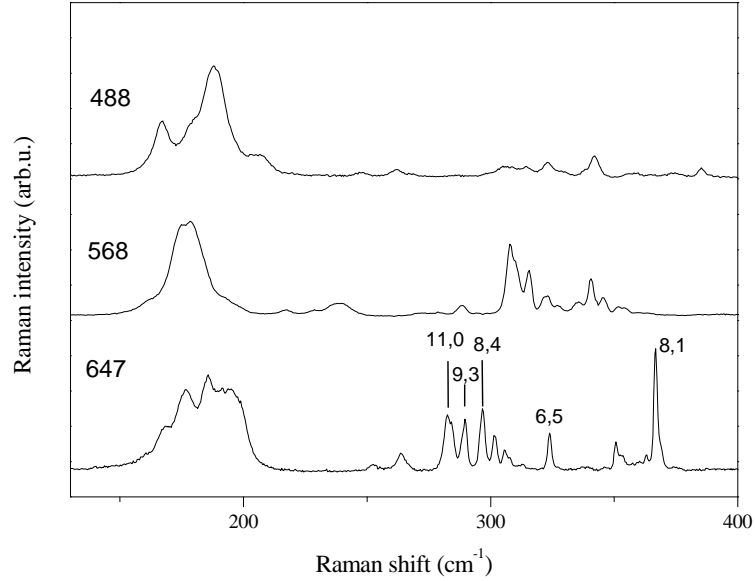


FIG. 7: Raman response of the RBM of a DWCNT sample when excited with different lasers. The spectra were recorded at 90 K. The indexing for some inner tube RBMs is shown for the $\lambda=647$ nm laser energy.

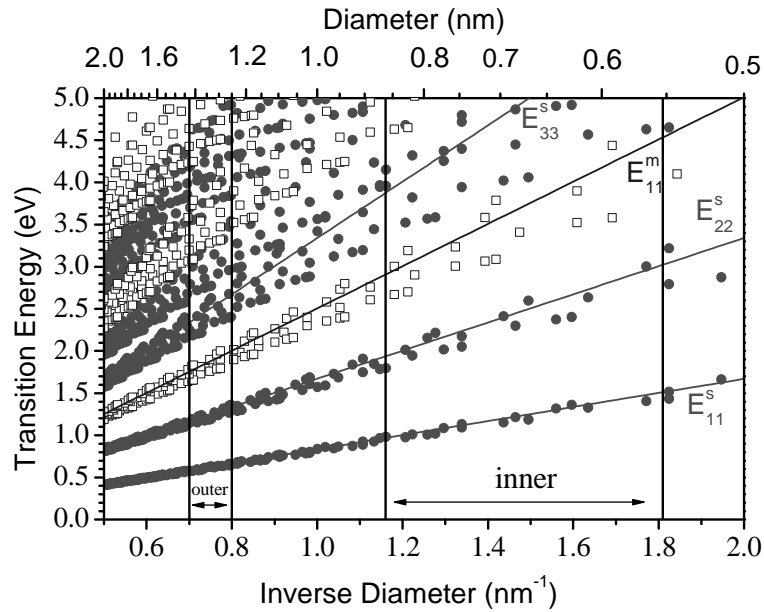


FIG. 8: Kataura plot with vertical lines indicating the diameter regions of inner and outer nanotubes that are relevant for the current study.

The Kataura plot that is relevant for the current study is shown in Fig. 8. It describes the relation between the optical transitions and the tube diameters. It shows that when using red laser excitations ($\gtrsim 2$ eV), nominally semiconducting inner tubes are expected to be observed. The metallic inner tubes are expected to appear only for higher energy excitations, above 2.5 eV.

The presence of metallic tubes, as e.g. the (9,3) inner tube at the 647 nm laser excitation in Fig. 7 is unexpected as they should only be observable at significantly larger excitation energy when resonance with the E_{11}^m transition occurs. This proves that smaller energy optical transitions are present for small diameter nanotubes that are absent in the simplest tight-binding calculations. Fig. 9 compares the zone folded tight-binding and *ab initio* derived density

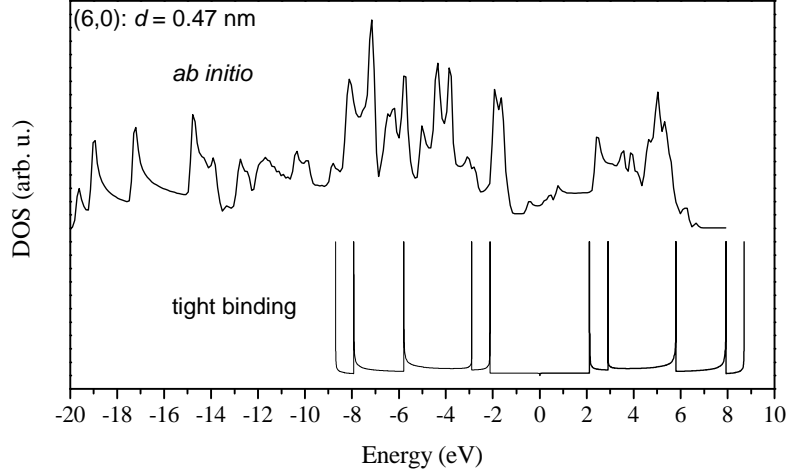


FIG. 9: Electronic density of states for a small diameter, metallic nanotube using *ab initio* and tight-binding techniques. The additional structure seen in the *ab initio* calculations between the two first Van Hove singularities of the tight-binding method gives rise to resonances at excitation energies lower than E_{11}^m .

of states (DOS) for a (6,0) metallic tube. The *ab initio* calculations show the presence of some structures between the lowest energy optical transitions of the tight-binding model, giving rise to the experimentally observed resonance. The observed difference between the *ab initio* and the tight-binding theory results from the finite curvature of the small diameter nanotubes. This curvature induces the mixing of the σ and the inward pointing π orbitals.

The width of the Van Hove singularities of the DOS of SWCNTs is a measure of their one-dimensional character. It can be measured from high resolution energy dispersive Raman studies. The results in the 700-750 nm excitation energy range are shown in Fig. 10. Dashed lines mark the Raman shift where the RBMs of two selected inner SWCNTs were followed for several laser excitations. The FWHM of the energy dependent inner tube intensities and thus the FWHM of the Van Hove singularities was found to be 60 meV [36]. This value is very small and reflects the one dimensional character of the SWCNTs. However, this does not significantly differ from values obtained from CVD grown, individual SWCNTs in a previous study [37]. This shows that the high perfectness of the inner tubes as deduced from the phonon lifetimes has no influence on the width of the singularities in their DOS as compared to the non defect-free outer SWCNTs. It rather supports the enhancement of electron-phonon coupling for small diameter nanotubes as the origin for the signal enhancement. If, however, an enhanced electron phonon coupling is present for the small diameter tubes, one expects a range of interesting physical phenomena to arise for the small tube such as Peierls transition [38] or superconductivity [39]. Indeed, superconductivity has been observed with a critical transition temperature of $T_c = 15$ K in 0.4 nm diameter SWCNTs [40]. However, the relevance of such phenomena for the inner tubes embedded in DWCNTs is not yet settled and is currently being investigated.

Splitting of the inner tube response of DWCNTs

In addition to the well defined number of geometrically allowed inner tubes, a larger number of RBMs are observed. In Fig. 11 we show spectra measured in the high resolution mode at the 647 nm laser excitation at 90 K. The spectra after deconvolution with the resolution of the spectrometer are also shown. The resolution of the spectrometer contributes to an additional Gaussian broadening of the intrinsically Lorentzian RBM lineshapes. The width of the Gaussian was measured from the response of our apparatus to the exciting laser and was found to be $0.4\text{-}0.7\text{ cm}^{-1}$ depending on the laser energy. The presence of additional, split components is apparent in Fig. 11 for some tubes. Some RBMs split into even 3 and more components. This splitting is a natural consequence of the different number of geometrically allowed inner and outer tubes and is related to the interaction between the two shells of the DWCNTs. As the diameters of both the inner and outer tubes are discrete sequences, some inner tubes can be grown in outer tubes with different diameters. Then the difference in inner-outer tube wall distance gives rise to a different interaction that causes the observed splitting of the lines. A rough estimate yields that for the DWCNTs studied here, 40 geometrically allowed outer tubes accommodate 20 geometrically allowed inner tubes. As a consequence, on

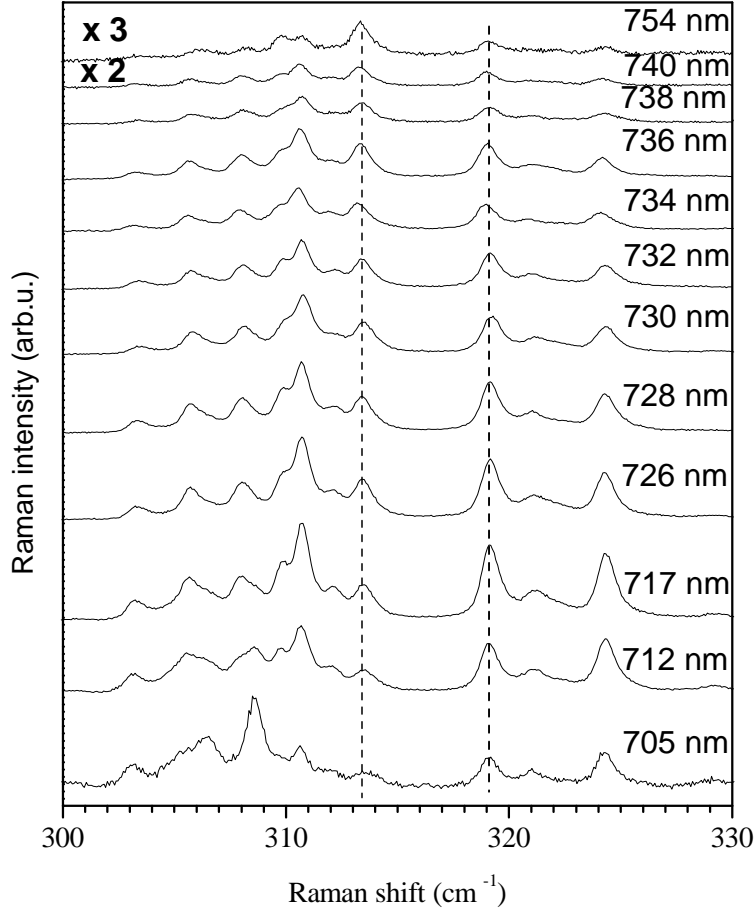


FIG. 10: Energy dispersive Raman spectra of the DWCNT sample in the 700-750 nm excitation energy range. Dashed lines indicate the same inner tube RBM followed for several laser excitations. The spectra are normalized to the incident power.

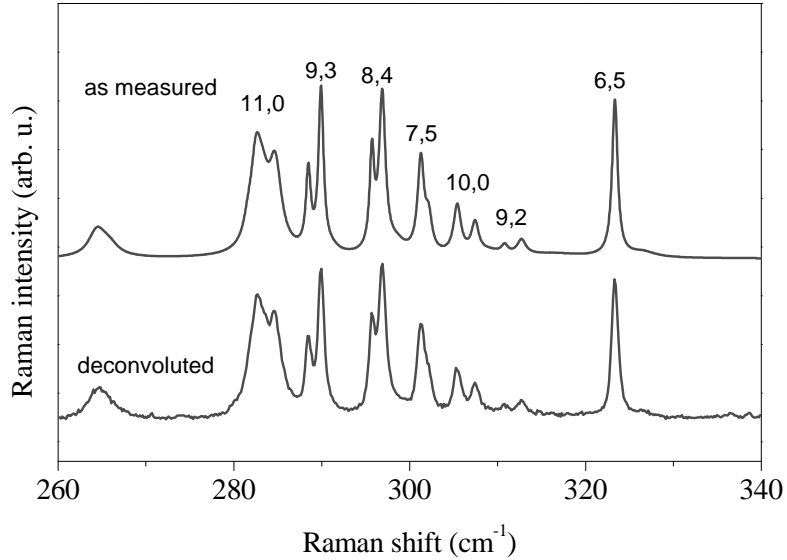


FIG. 11: High resolution Raman spectra of inner tube RBMs of DWCNT at $\lambda=647$ nm laser excitation and 90 K. We also show the corresponding spectrum after deconvolution with the resolution of the spectrometer.

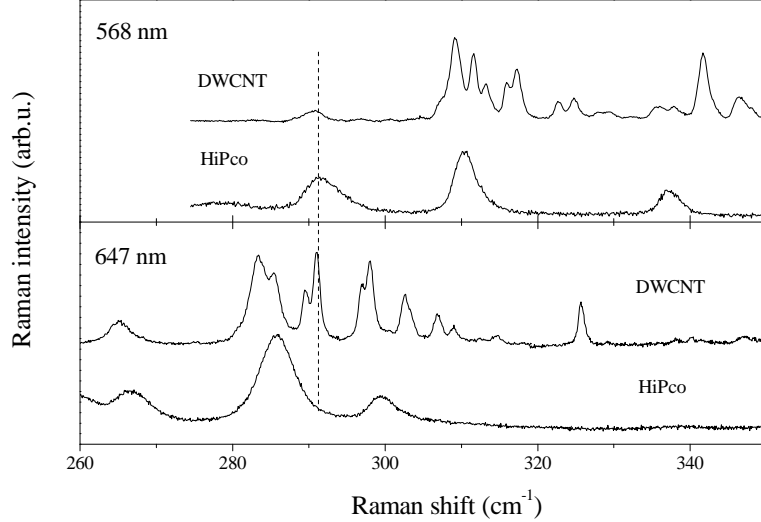


FIG. 12: Comparison of the inner tube RBMs of a DWCNT sample and the RBMs of a sample prepared by the HiPco process at $\lambda=568$ nm and 647 nm laser energy. Both samples were measured at 90 K in the high resolution mode.

average splitting into two components is expected. This estimate, however, does not account for the magnitude of the splitting that is currently being further investigated both experimentally and theoretically [41].

In addition to the two-wall related splitting of the RBMs of inner tubes, further peculiarities can be observed. In Fig. 12 we compare the inner tube RBMs of a DWCNT sample with the RBMs of a small diameter SWCNT sample. The latter was a HiPco sample with a mean diameter and a variance of $d = 1.05$ nm and $\sigma = 0.15$ nm, respectively [42]. The figure shows this comparison for 568 nm and 647 nm laser excitation. The larger number of RBMs in the DWCNT sample as compared to the HiPco sample and the absence of splitting for the RBMs in the HiPco sample is observed. Broader RBM lines are observed in the HiPco sample, however this would not limit the observation of the splitting. As discussed above, the splitting is related to the two-shell nature of the DWCNT samples and thus its absence is natural in the HiPco sample. However, the absence of some RBMs corresponding to geometrically allowed tubes in the HiPco sample that are observed in the inner tube DWCNT spectrum is intriguing. The absence of geometrically allowed SWCNTs or the smaller number of optical transitions in the HiPco samples may explain for our observation. The dashed line in Fig. 12 shows an example for a tube RBM that is absent at 647 nm excitation from the HiPco spectrum, however appears at 568 nm excitation. Similar behavior was observed for other, missing HiPco RBM modes, i.e. the RBM modes of the SWCNTs of the HiPco samples are also present, although at much less number of laser lines. This clearly shows, that all the geometrically allowed SWCNTs are present both among the inner tubes and also in the HiPco sample, however, there is a significantly larger number of optical transitions for the inner tubes of the DWCNT sample. This is most probably related to a yet unexplained intricate interplay between the two shells of the DWCNT samples and calls for theoretical work on this issue. In addition to the larger number of lines observed in the inner tube RBM spectrum of DWCNTs, a slight downshift ranging from 2-3 cm^{-1} is also observed. This downshift is related to the different environment for an inner tube of the DWCNT and for an SWCNT in a HiPco sample. The earlier is surrounded by an outer tube, whereas the latter is embedded in bundles. These interactions give rise to a different value for the C_2 constant of the RBM mode frequencies. The broader linewidths observed in the HiPco sample underlines the highly perfect nature of the inner nanotubes.

Chiral index assigment for inner tubes

The reciprocal relation between the RBM frequencies and the tube diameters contributes to a significant spectral spread for the observed inner tube RBMs. This, together with the narrow linewidths observed for the inner tubes allows the accurate (n, m) indexing of the tubes. In Fig. 13, the inner tube RBMs measured at several laser lines are shown. The observation of a large number of well defined RBMs allows the determination of RBM shifts corresponding to distinct inner tubes. The Raman shifts of observable inner tubes are summarized in Table. I, together with the

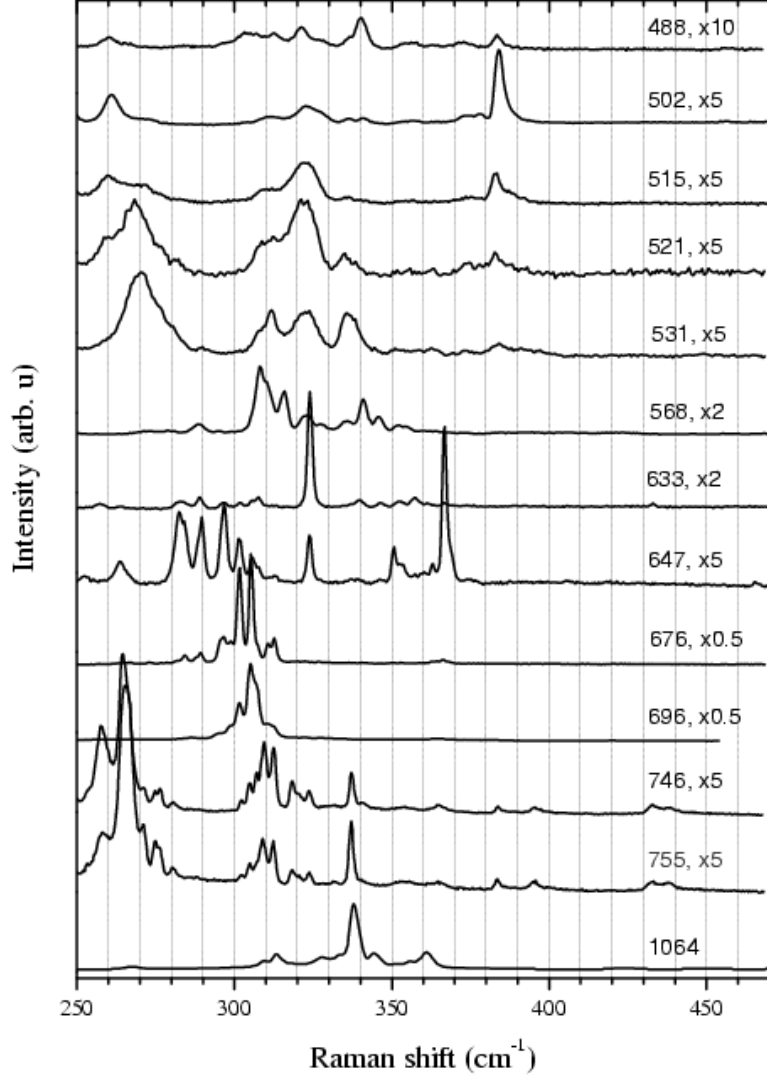


FIG. 13: DWCNT RBM spectra measured at 90 K for several laser excitations.

assigned chiral vectors, and tube diameters calculated with DFT methods. It was found that the diameters of small tubes, based on the lattice constant of graphene gives significant deviations as compared to the DFT calculated tube diameters [43].

In Fig. 14 we compare the inverse tube diameters calculated from the lattice constant of graphene and from a DFT calculation. A simple interpolation could be established: $1/d_{\text{DFT}} = 1/d_G - (0.0050/d_G^2 + 0.0013/d_G^4)$, where d_{DFT} and d_G are the DFT and the graphene derived tube diameters, respectively, and d_G is expressed from the chiral indices as: $d_G = 0.141\sqrt{3}(m^2 + n^2 + mn)/\pi$. The C_1 and C_2 constants of the RBM frequencies $\nu_{\text{RBM}} = C_1/d_{\text{DFT}} + C_2$ were determined from a linear regression and $C_1 = 233 \text{ cm}^{-1} \text{ nm}$ and $C_2 = 14 \text{ cm}^{-1}$ were found. Fig. 15 shows that no linear relationship could be established between the RBM frequencies and the graphene derived inverse tube diameters. However, a very reliable fit is obtained with small discrepancies between calculated and measured RBM frequency values when the DFT optimized tube diameters were used. It establishes that the reciprocal relationship between the RBM frequencies and the tube diameters, when the latter is properly calculated, is valid down to the smallest observable inner tubes. The value determined for the C_1 constant is not restricted to small diameter tubes only, however studies on larger diameter tubes have been lacking the precision that could be obtained from the inner tube analysis of DWCNTs. Therefore a direct comparison with previously determined values can not be performed. It has been pointed out above that the different environment for an inner tube and for an SWCNT in a bundle prevents a comparison of the respective C_2 parameters.

TABLE I: Inner tube RBM frequencies and tube diameters: (1) center of gravity line position of the RBM averaged from different laser excitations, (2) CNT chiral indices, (3) interpolated DFT determined tube diameters, (4) first and second tight-binding optical transition energies with $\gamma_0 = 2.9$ eV, (5) theoretical RBM frequencies at the best fit with $C_1 = 233 \text{ cm}^{-1} \text{ nm}$ and $C_2 = 14 \text{ cm}^{-1}$. ("n.i.": not identified), from [43].

ν_{RBM} expt. (cm^{-1})	Chirality (n,m)	d_{RBM} (nm)	E_{11}/E_{22} (eV)	$\nu_{\text{RBM}}^{\text{theor.}}$ (cm^{-1})
246.1	(11,3)	0.997	0.84/1.59	247.8
252.4	(12,1)	0.978	0.86/1.60	252.1
n.i.	(10,4)	0.975	2.36/4.21	252.9
257.6	(9,5)	0.960	0.84/1.73	256.8
260.5	(8,6)	0.950	0.87/1.69	259.2
n.i.	(11,2)	0.947	2.40/4.24	260
n.i.	(7,7)	0.947	2.52/4.54	260
n.i.	(12,0)	0.937	2.40/4.25	262.6
265.3	(10,3)	0.921	0.87/1.84	267
270.5	(11,1)	0.901	0.85/1.91	272.5
274.7	(9,4)	0.901	0.82/1.75	272.5
n.i.	(8,5)	0.888	2.61/4.60	276.5
280.2	(7,6)	0.881	0.93/1.85	278.5
282.3	(10,2)	0.871	0.97/1.78	281.6
284.0	(11,0)	0.860	0.98/1.80	284.9
289.1	(9,3)	0.846	2.67/4.63	289.4
296.1	(8,4)	0.828	0.98/2.00	295.4
298.9	(10,1)	0.824	2.70/4.65	296.7
301.9	(7,5)	0.817	1.01/1.95	299.2
304.0	(6,6)	0.813	2.90/5.02	300.5
306.5	(9,2)	0.794	1.01/2.15	307.3
311.7	(10,0)	0.783	1.02/2.22	311.6
317.2	(8,3)	0.771	1.09/2.02	316.1
319.8	(7,4)	0.756	3.00/5.07	322.5
323.0	(9,1)	0.748	1.13/2.05	325.8
327.9	(6,5)	0.748	1.09/2.17	325.8
336.7	(8,2)	0.719	3.06/5.09	338.3
340.3	(9,0)	0.706	3.08/5.10	344.1
345.8	(7,3)	0.697	1.15/2.41	348.2
353.8	(6,4)	0.684	1.21/2.30	354.6
358.5	(5,5)	0.680	3.37/5.52	356.8
364.9	(8,1)	0.671	1.19/2.60	361.4
374.5	(7,2)	0.643	1.32/2.38	376.3
383.5	(8,0)	0.629	1.36/2.40	384.4
389.3	(6,3)	0.624	3.52/5.54	387.3
395.6	(5,4)	0.615	1.33/2.63	393.2
405.8	(7,1)	0.595	3.58/5.55	405.9
422.0	(6,2)	0.569	1.40/3.00	423.8
432.9	(7,0)	0.553	1.43/3.22	435.7
438.1	(5,3)	0.553	1.52/2.79	435.7
444.5	(4,4)	0.547	4.10/5.80	439.9
462.1	(6,1)	0.519	1.66/2.87	463.1

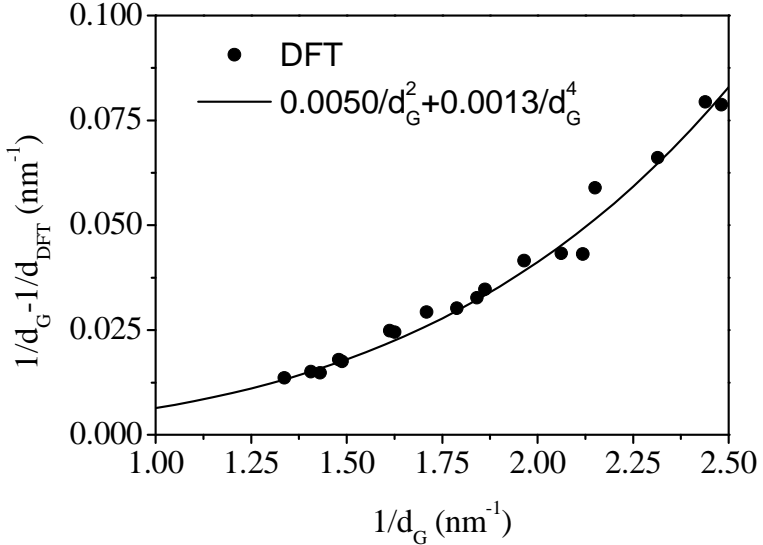


FIG. 14: Difference between graphene and DFT derived inverse tube diameters. The solid line is a polynomial interpolation.

In conclusion, the Raman studies of peapod based DWCNT materials have been reviewed. It was shown that this material has an unprecedently high perfectness related to the growth in the catalyst free environment. The growth mechanism is not fully understood and some alternative mechanisms have been discussed. A method is presented that enables the industrial scaling up of the DWCNT production. The properties of the DWCNT have been compared with a similar diameter SWCNT material, a HiPco sample. The geometrically allowed small diameter tubes are present in both materials. However, due to the smaller number of optical transitions in the HiPco sample, a smaller number of RBM lines are observed. A splitting of the geometrically allowed inner tube RBMs in the DWCNT sample was observed. It was explained by the different shell-shell distance of inner-outer tube pairs with varying diameters. The sharp appearance of the inner tube RBMs and their relatively larger spectral spread allowed a chiral index assignment for a broad spectral range and Raman shifts. It was found that a linear relation could be established between the RBM frequencies and DFT determined tube diameters. The empirical constants relating the RBM frequencies and the tube diameters have been refined. Nevertheless, a direct comparison with values determined on free-standing or bundled SWCNTs is not straightforward.

ACKNOWLEDGEMENTS

The authors gratefully acknowledge J. Kürti, and V. Zólyomi for many fruitful discussions and for the DFT calculations. H. Kataura is acknowledged for providing some of the C₆₀ peapod materials. We thank Hui-Ming Cheng for providing the CVD grown DWCNT sample. The authors gratefully acknowledge J. Bernardi for the TEM micrographs, Th. Pichler and Á. Kukovecz for their contributions to the Raman experiments. This work was supported by the Austrian Science Funds (FWF) project Nr. 14893 and by the EU projects NANOTEMP BIN2-2001-00580 and PATONN Marie-Curie MEIF-CT-2003-501099.

[1] S. Iijima, *Nature (London)* **354**, 56 (1991).
[2] J. H. Hafner, C. L. Cheung, C. M. Lieber, *Nature* **398**, 761 (1999).
[3] G. Z. Yue, Q. Qiu, B. Gao, Y. Cheng, J. Zhang, H. Shimoda, S. Chang, J. P. Lu, and O. Zhou, *Appl. Phys. Lett.* **81**, 355 (2002).
[4] A. N. Obraztsov, I. Pavlovsky, A. P. Volkov, E. D. Obraztsova, A. L. Chuvilin, V. L. Kuznetsov, *J. Vac. Sci. and Techn. B* **18**, 1059 (2000).
[5] M. S. Dresselhaus, G. Dresselhaus, P. C. Ecklund: *Science of Fullerenes and Carbon Nanotubes*, Academic Press, San Diego 1996.

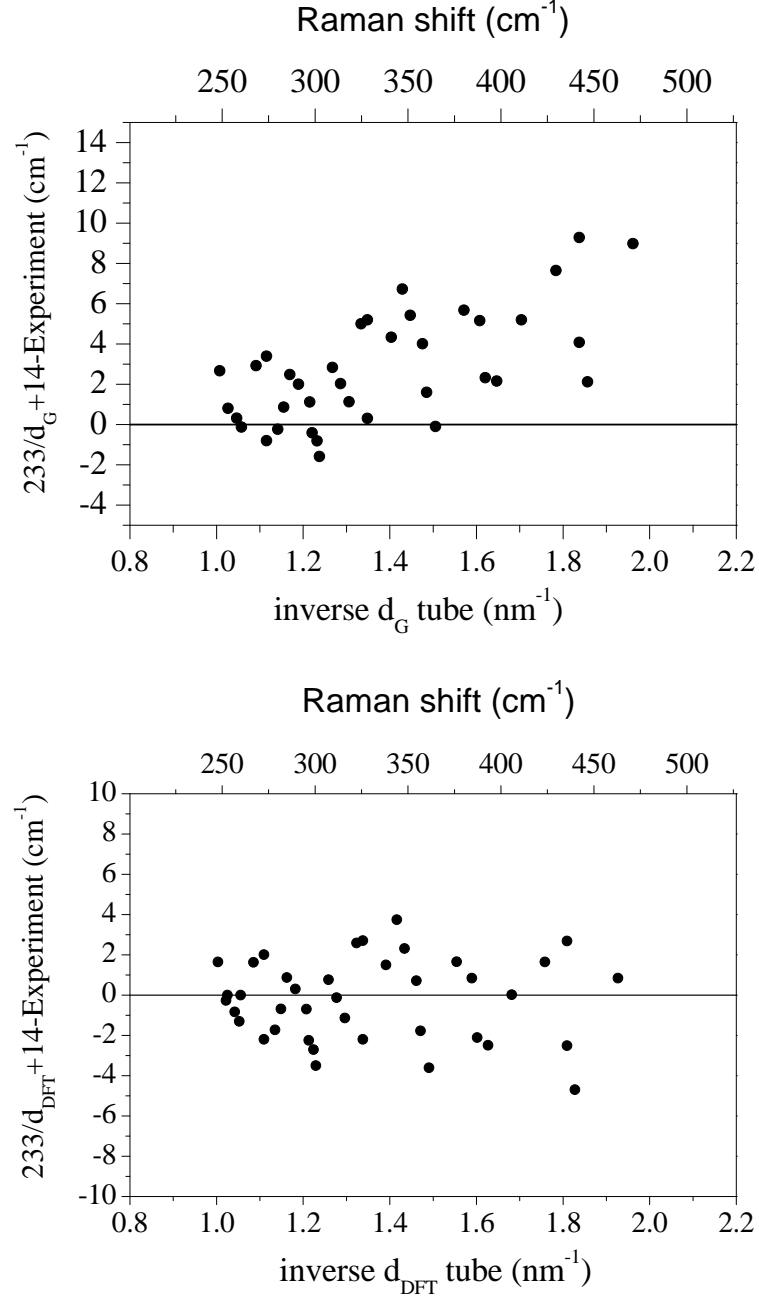


FIG. 15: Difference between the calculated and measured RBM Raman shifts when the graphene derived (upper panel) and DFT optimized (lower panel) tube diameters were used.

- [6] D. Chattopadhyay, L. Galeska, and F. Papadimitrakopoulos F, J. Am. Chem. Soc. **125**, 3370 (2003).
- [7] R. Krupke, F. Hennrich, H. von Lohneysen, and M. M. Kappes, Science **301**, 344 (2003).
- [8] Z. H. Chen, X. Du, M. H. Du, C. D. Rancken, H. P. Cheng, and A. G. Rinzler, Nano Lett. **3**, 1245 (2003).
- [9] M. Zheng, A. Jagota, M. S. Strano, A. P. Santos, P. Barone, S. G. Chou, B. A. Diner, M. S. Dresselhaus, R. S. McLean, G. B. Onoa, G. G. Samsonidze, E. D. Semke, M. Usrey, and D. J. Walls, Science **302**, 1545 (2003).
- [10] M. J. O'Connell, S. M. Bachilo, C. B. Huffman, V. C. Moore, M. S. Strano, E. H. Haroz, K. L. Rialon, P. J. Boul, W. H. Noon, C. Kittrell, J. P. Ma, R. H. Hauge, R. B. Weisman, and R. E. Smalley, Science **297**, 593 (2002).
- [11] B. W. Smith, M. Monthioux, and D. E. Luzzi, Chem. Phys. Lett. **315** 31 (1999).
- [12] B. W. Smith, M. Monthioux, and D. E. Luzzi, Nature **396**, 323 (1998).
- [13] H. Kataura, Y. Maniwa, T. Kodama, K. Kikuchi, K. Hirahara, K. Suenaga, S. Iijima, S. Suzuki, Y. Achiba, W. Krätschmer, Synth. Met. **121**, 1195 (2001).

- [14] S. Bandow, M. Takizaw, K. Hirahara, M. Yudasaka, and S. Iijima, *Chem. Phys. Lett.* **337** 48 (2001).
- [15] J. L. Hutchison, N. A. Kiselev, E. P. Krinichnaya, A. V. Krestinin, R. O. Loutfy, A. P. Morawsky, V. E. Muradyan, E. D. Obraztsova, J. Sloan, S. V. Terekhov, and D. N. Zakharov, *Carbon* **39**, 761 (2001).
- [16] Wencai Ren, Feng Li, Jian Chen, Shuo Bai, and Hui-Ming Cheng, *Chem. Phys. Lett.* **359**, 196 (2002).
- [17] H. Kuzmany, W. Plank, M. Hulman, C. Kramberger, A. Gruneis, T. Pichler, H. Peterlik, H. Kataura, and Y. Achiba, *Eur. Phys. J. B* **22**, (2001) 307.
- [18] X. Liu, T. Pichler, M. Knupfer, M. S. Golden, J. Fink, H. Kataura, Y. Achiba, K. Hirahara, and S. Iijima, *Phys. Rev. B* **65** (2002) 045419.
- [19] G. Kresse and D. Joubert, *Phys. Rev. B* **59** 1758 (1999).
- [20] B. W. Smith, and D. E. Luzzi, *Chem. Phys. Lett.* **321** 169 (1999).
- [21] M. Abe, H. Kataura, H. Kira, T. Kodama, S. Suzuki, Y. Achiba, K. Kato, M. Takata, A. Fujiwara, K. Matsuda, and Y. Maniwa, *Phys. Rev. B* **68**, 041405 (2003).
- [22] M. Melle-Franco, H. Kuzmany, and F. Zerbetto, *J. Phys. Chem. B* **109**, 6986 (2003).
- [23] S. Berber, Y-K. Kwon, D. Tománek, *Phys. Rev. Lett.* **88**, 185502 (2002).
- [24] A. Rochelefort, cond-mat/0301310.
- [25] R. Pfeiffer, H. Kuzmany, C. Kramberger, C. Schaman, T. Pichler, H. Kataura, Y. Achiba, J. Kürti, and V. Zólyomi, *Phys. Rev. Lett.* **90**, 225501 (2003).
- [26] M. Holzwebver, Ch. Kramberger, F. Simon, Á. Kukovecz, H. Kuzmany, and H. Kataura in the Proceedings of the XVII International Winterschool on Electronic Properties of Novel Materials, edited by H. Kuzmany, J. Fink, M. Mehring, and S. Roth, AIP Publishing, New York, 2003, p. 306.
- [27] S. Bandow, T. Hiraoka, T. Yumura, K. Hirahara, H. Shinohara, and S. Iijima, *Chem. Phys. Lett.* **384**, 320 (2004).
- [28] D. Tománek, private communication.
- [29] Y. Zhao, B. I. Yakobson, R. E. Smalley, *Phys. Rev. Lett.* **88**, 185501 (2002).
- [30] K. Hirahara, S. Bandow, K. Suenaga, H. Kato, T. Okazaki, H. Shinohara, and S. Iijima, *Phys. Rev. B* **64**, 115420 (2001).
- [31] F. Simon *et al.*, unpublished.
- [32] F. Simon, H. Kuzmany, H. Rauf, T. Pichler, J. Bernardi, H. Peterlik, L. Korecz, F. Fülöp, and A. Jánossy, *Chem. Phys. Lett.* **383**, 362 (2004).
- [33] Feng Li, S. G. Chou, Wencai Ren, J. A. Gardecki, A. K. Swan, M. S. Ünlü, B. B. Goldberg, Hui-Ming Cheng, and M. S. Dresselhaus, *J. Mater. Res.* **18**, 1251 (2003).
- [34] A. Jorio, R. Saito, J. H. Hafner, C. M. Lieber, M. Hunter, T. McClure, G. Dresselhaus, and M. S. Dresselhaus, *Phys. Rev. Lett.* **86**, 1118 (2001).
- [35] M. Machón, S. Reich, J. M. Pruneda, C. Thomsen, and P. Ordejón in the Proceedings of the XVII International Winterschool on Electronic Properties of Novel Materials, edited by H. Kuzmany, J. Fink, M. Mehring, and S. Roth, AIP Publishing, New York, 2003, p. 427.
- [36] A. Sen, Ch. Kramberger, Ch. Schaman, R. Pfeiffer, H. Kuzmany, and H. Kataura in the Proceedings of the XVII International Winterschool on Electronic Properties of Novel Materials, edited by H. Kuzmany, J. Fink, M. Mehring, and S. Roth, AIP Publishing, New York, 2003, p. 314.
- [37] A. Jorio, A. G. Souza, G. Dresselhaus, M. S. Dresselhaus, R. Saito, J. H. Hafner, C. M. Lieber, F. M. Matinaga, M. S. S. Dantas, and M. A. Pimenta, *Phys. Rev. B* **63**, 245416 (2001).
- [38] George Grüner: Density waves in solids, Addison-Wesley Publishing Company, 1994.
- [39] Michael Tinkham: Introduction to superconductivity, Krieger Publishing Company, 1975.
- [40] Z. K. Tang, L. Y. Zhang, N. Wang, X. X. Zhang, G. H. Wen, G. D. Li, J. N. Wang, C. T. Chan, and P. Sheng, *Science* **292** 2462 (2001).
- [41] R. Pfeiffer, *et al.* unpublished.
- [42] Á. Kukovecz, Ch. Kramberger, V. Georgakilas, M. Prato, and H. Kuzmany, *Eur. Phys. J. B* **28**, 223 (2002).
- [43] Ch. Kramberger, R. Pfeiffer, H. Kuzmany, V. Zólyomi, and J. Kürti, *Phys. Rev. B* **68**, 235404 (2003).